Mitochondrially Targeted Gene Therapy Rescues Visual Loss in a Mouse Model of Leber's Hereditary Optic Neuropathy

Tsung-Han Chou , Zixuan Hao , Diego Alba , Angelina Lazo , Gabriele Gallo Afflitto , Jeremy D Eastwood , Vittorio Porciatti * , John Guy , Hong Yu *

Posted Date: 28 September 2023

doi: 10.20944/preprints202309.1961.v1

Keywords: LHON; MTSAAV; human ND4; gene therapy

Article

Mitochondrially Targeted Gene Therapy Rescues Visual Loss in a Mouse Model of Leber's Hereditary Optic Neuropathy

Tsung-Han Chou [1], Zixuan Hao [1], Diego Alba [1], Angelina Lazo [1], Gabriele Gallo Afflitto [1], Jeremy D. Eastwood [1], Vittorio Porciatti [1,*], John Guy [1] and Hong Yu [1,*]

[1] Bascom Palmer Eye Institute, University of Miami Miller School of Medicine, Miami, FL, USA

* Correspondence: vporciatti@med.miami.edu (V.P.) and hyu3@med.miami.edu (H.Y.)

Abstract: Leber's hereditary optic neuropathy (LHON) is a common mitochondrial genetic disease, causing irreversible blindness in young individuals. Current treatments are inadequate, and there is no definitive cure. This study evaluates the effectiveness of delivering wildtype human NADH ubiquinone oxidoreductase subunit 4 (hND4) gene using mito-targeted AAV(MTSAAV) to rescue LHOH mice. We observed declining pattern electroretinograms amplitudes as mice aged across all groups (P< 0.001), with significant differences among groups (P = 0.023, Control vs. LHON, P = 0.008; Control vs. Rescue, P = 0.228). Inner retinal thickness and intraocular pressure do not change significantly with age or groups. Compared to LHON mice, those rescued with wildtype hND4 exhibit improved retinal visual acuity (0.29± 0.1 cy/deg vs.0.15 ± 0.1 cy/deg) and increased functional hyperemia response (effect of flicker, P<0.001, effect of Group, P=0.004; Interaction Flicker x Group, P<0.001). Postmortem analysis shows a marked reduction in retinal ganglion cell density in the LHON group compared to the other groups (Effect of Group, P<0.001, Control vs. LHON, P<0.001, Control vs. Rescue, P=0.106). These results suggest that MTSAAV-delivered wildtype hND4 gene rescues, at least in part, visual impairment in an LHON mouse model and has the therapeutic potential to treat this disease.

Keywords: LHON; MTSAAV; human ND4; gene therapy

1. Introduction

Mitochondrial dysfunction underlies a large number of diseases and aging process [1]. Many mitochondrial-related disorders are the result of point mutations or deletions in the mitochondrial genome. Among these, Leber Hereditary Optic Neuropathy (LHON) stands out as the most common primary mitochondrial genetic disease. It manifests as sudden, severe, and irreversible vison loss, predominantly affecting children and young adults. More than 90% of LHON cases are caused by one of the three point mutations in the mitochondrial DNA (mtDNA): m. 11778 G>A, m.3460G>A, and m.14484 T>C. These mutations respectively affect subunits ND4, ND1, and ND6, which are crucial components of the respiration complex I [2,3].

Pharmacological therapies for LHON, much like in other mitochondrial diseases, have proven to be insufficient, and there is no FDA approved-therapy available, currently. Gene therapy approaches have been explored as potential treatment options for LHON [4–6]. Among these approaches, allotopic expression has advanced to human testing specifically for m. 11778G>A mutation. Clinical trials for this approach are being conducted in China (NCT01267422) [7], France (NCT02064569) [8], and the USA (NCT02161380) [9,10], with the French trial currently in phase 3 trials and being conducted in the USA and Europe. While these clinical trials have shown some degree of visual improvement in LHON patients, most participants in the study cohorts still suffer from low vision and remain legally blind, particularly those who have experienced vison loss for over a year. As a result, new and innovative approaches are needed to enhance treatment outcomes for LHON patients and provide more significant visual recovery.

Viruses have the ability to traverse the mitochondrial double membrane to access the inner matrix and deliver DNA inside the organelle [11]. Yu et al. have demonstrated that fusing a

 doi:10.20944/preprints202309.1961.v1

mitochondrial targeting sequence (MTS) to the capsid of adeno-associated virus (MTS-AAV) can redirect the virus to mitochondria rather than the nucleus [12]. Using the MTS-AAV, we successfully delivered the wild type human ND4 gene to LHON cybrids homoplasmic for m.11778G>A mutation and rescued the cells from defective respiration [5]. We also explored its potential in the adult rodent visual system, where it effectively prevented visual loss and optic nerve atrophy induced by the mutant R340H ND4 [5,13].

Our subsequent studies further demonstrated the versatility of this approach. Introducing the mutant hND4 gene into mouse zygotes, we generated bona fide LHON mitomice carrying human m.11778G>A mutation. The translated hND4 protein assembled into host respiratory complexes, leading to decreased respiratory chain function, and increased oxidative stress. This mitomice model accurately recapitulated the progressive loss of retinal ganglion cells (RGCs) and optic nerve degeneration observed in the human form of LHON [14]. In a more recent study, we used the same approach to deliver human ND1/m. 3460G>A [15] and ND6/m.14484T>C [16] into mouse eyes, respectively. The delivered gene induced visual and RGC loss in the mice. Importantly, our findings revealed that the mitochondrially delivered DNA showed superior efficacy in rescuing LHON mice compared to allotopic ND4 delivery [17].

In this study, we conducted an extension to comprehensively assess the rescue effects of MTSAAV-delivered wild-type ND4 in LHON mice, including flicker-induced changes in retinal ganglion cell function, pattern visual evoked potential, and mitochondria integrity. These studies are part of our preclinical testing of MTSAAV-delivered ND4, and the results obtained from this research will help to gain regulatory approval for this therapy for future human testing.

2. Materials and Methods

2.1. Plasmids and AAVs

sc-HSPCSB-hND4-mCherry was constructed as previously described [5,14]. In brief, human *ND4* gene was fused in frame with *FLAG*, and mitochondrial-encoded *Cherry*(mCherry) were cloned into scAAV backbones under the control of the mitochondrial heavy strand promoter (HSP) including 3 upstream conserved sequence blocks (*HSPCSB*), where *ND4FLAG* is followed by *mCherry* with a stop codon between two genes. *mCherry* cloned in the same scAAV backbone was used as a control (sc-HSPCSB-mCherry). Mutant human *ND4G11778A* gene was cloned into the same AAV backbone under the control of HSP (sc-HSP-hND4G11778A-mCherry) and used for making LHON mouse model. The resultant plasmids were purified using Qiagen endotoxin free maxiprep and then packaged with the *VP2COX8* plus *VP1*, *VP3* and helper plasmid PXX6 into recombinant virus: MTSAAV/hND4-mCherry, MTSAAV/mCherry, and MTSAAV/hND4G11778A-mCherry.

2.2. Animals and intravitreal injections (IVI)

All animal procedures were performed abiding by the National Institutes of Health Guide for Care and Use of Laboratory Animals and the ARVO Statement for the use of Animals in Ophthalmic and Vision Research. 3-month-old DBA/1J (D1) mice (N =60) were sedated by the IP injection of ketamine (100mg/ml, 1.5 ml), xylazine (20 mg/ml, 1.5 ml), injectable water (7 ml) mixture for the pattern electroretinograms (PERG), flash electroretinograms (FERG), spectral-domain optical coherence tomography (SD-OCT) baseline recordings. After the PERG baseline recordings, we randomized the mice into three groups (N=20 per group) to make the averaged PERG similar between the groups. Then we delivered intravitreally the MTSAAV/hND4G11778A-mCherry (6 E9 vg/eye) into both eyes in 40 D1 mice and divided them randomly into LHON (N=20) and rescue (N=20) groups. The LHON group (N=20) received MTSAAV/mCherry (6 E9 vg/eye), and the rescue group (N=20) received MTSAAV/ hND4-mCherry (6 E9 vg/eye). A control group (N=20) received two IVI of MTSAAV/mCherry (6 E9 vg/eye).

2.3. PERG, FERG, and SD-OCT

Preprints (www.preprints.org) | NOT PEER-REVIEWED | Posted: 28 September 2023 doi:10.20944/preprints202309.1961.v1

RGC function was assessed by Pattern Electroretinogram (PERG) [18], using a commercially available instrument (Jorvec Corp. FL, USA) to simultaneously record responses from both eyes as previously described in detail [19,20]. In brief, Ketamine/Xylazine anesthetized mice were gently restrained in a holder allowing unobstructed vision and kept at a constant body temperature of 37.0 °C using feedback-controlled heating pad controlled by a rectal probe. Pupils were undilated and small (<1 mm), which insured a large depth of focus. PERG signals were recorded from a subcutaneous stainless-steel needle (Grass, West Warwick, RI, USA) placed in the snout. The reference and ground electrodes were similar needles placed medially on the back of the head and at the root of the tail, respectively. Visual stimuli were presented at each eye independently from 10 cm distance and consisted of contrast-reversal of gratings (0.05 cycles/deg, 98% contrast) generated on two light-emitting diode (LED) tablets (15 × 15 cm square field, 800 cd/m² mean luminance) alternating at slightly different frequencies around 1 Hz (OD, 1.016 Hz; OS, 1.008 Hz). Independent PERG signals from each eye were retrieved using one channel continuous acquisition and phase-locking average over 372 epochs for each eye. PERG amplitude was measured peak-to-trough using a software that automatically detected the positive peak and the negative trough in the PERG waveform (typically the P1 peak to the N2 trough). Noise responses were obtained by computing the difference between even and odd epochs [14].

To have a corresponding index of outer retinal function, a light-adapted flash Electroretinogram (FERG) was also recorded with undilated pupils in response to strobe flashes of 20 cd/m²/s superimposed on a steady background light of 12 cd/m² and presented within a Ganzfeld bowl. Under these conditions, rod activity is largely suppressed while cone activity is minimally suppressed.

Retinal images were visualized with Heidelberg spectral-domain optical coherence tomography (SD-OCT) respectively. After the OCT images were taken, we used the IOWA Reference Algorithms OCT Explore software (Version 3.8.0) to quantitatively analyze the mouse retina layer of thickness [21,22].

2.4. PERG-based Visual acuity

Retinal visual acuity in mice were measured when they are 12-month-old by semi-automatic PERG recordings with multiple trials in different spatial frequencies. The peak-to-trough (P1 to N2) PERG amplitudes at different spatial frequencies were automatically measured together with the background noise. The PERG amplitude typically decreases with increasing spatial frequency. The PERG acuity was calculated by extrapolating PERG amplitude to the noise level [23] .

2.5. Flicker-induced PERG adaptation

To assess the effect of flicker on PERG, a flickering field was superimposed to the patterned stimulus as previously described [24] (inset figure). The patterned LED display was surrounded by a LED square frame (internal size 15 × 15 cm, external size 18 × 18 cm) to generate flickering light. The flickering frame had the same mean luminance of the patterned field, and could be modulated (square-wave, 50% duty cycle) at either 101 Hz or 11 Hz at constant mean luminance. These frequencies were asynchronous with the pattern reversal frequencies and did not contribute to the PERG waveform. At 101 Hz, flickering light could not be perceived by human observers. PERG + 101 Hz flicker (baseline) and PERG +11 Hz flicker (test) were recorded in sequence.

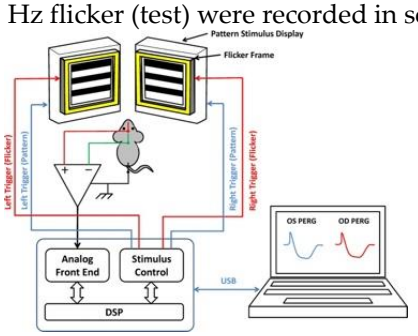

 doi:10.20944/preprints202309.1961.v1

2.6. Immunostaining

At 15-month-old, mouse retinas were harvested for RGC counting (RBPMS immunostaining) and mouse optic nerves were harvested for axon counting and axon mitochondria scoring (Transmission Electron Microscopy, TEM). Scoring axon and mitochondria is measured by double-blinded observers with three score system (healthy, mild, severe status).

2.7. Statistical Analysis

Data analysis was performed using Generalized Estimating Equation (GEE, IBM SPSS statistics Ver. 26), an unbiased non-parametric method to analyze longitudinal correlated data that also accounts for inclusion of multiple measurements from the same subject [25,26].

In the longitudinal analyses, dependent variables were PERG, FERG, IOP, and OCT, and predictor variables were age (3, 6, 9, 12, 15 month) and treatment group (Control, LHON, Rescue). Main effects (age, group) and interaction between age and group were computed, as well as pairwise combinations between age and group. An additional longitudinal group of naïve mice (3, 9, 16 months of age, n=4) was included for comparison but not incorporated in the GEE main analysis.

3. Results

3.1. Wild-type hND4 rescues RGC dysfunction induced by mutant hND4

RGCs are highly susceptible in patients with LHON mutations, we therefore want to assess whether MTSAAV-delivered wild type *hND4* gene could effectively counteract RGC dysfunction induced by mutant *hND4* allele. We conducted the study using 60 DBA/1J mice aged 3 months, which were randomly divided into three groups with 20 mice per group. As illustrated in Figure 1A, two of the groups were injected with MTSAAV/hND4G11778A-mCherry into the vitreous, inducing LHON phenotype. The third group served as a control (Control) and received MTSAAV/mCherry injections. Two days later, one of the LHON groups was treated with MTSAAV/hND4-mCherry to rescue the phenotype (Rescue), while the other LHON group received MTSAAV/mCherry as a disease control (LHON). For the control group (Control), we performed a second injection of MTSAAV/mCherry. Additionally, we included a group of mice that were not injected with any substances as a naïve control (Naïve, n=4).

As the first step, we wanted to detect whether double injections had any discernible impact on intraocular pressure (IOP). We observed significant age-related changes in IOP in all four groups of mice (Factor age, $P<0.01$). However, these changes were relatively small, ranging from approximately 3 to 5 mmHg. There were no significant differences between the groups (Factor group, $P=0.76$; Age x Group, $P=0.26$). Importantly, the IOP changes observed over time were within the range of normal physiological variations seen in naïve mice, suggesting that the double injections did not cause abnormal or extreme fluctuations in IOP levels (Figure 1B).

Considering that the visual pathway begins with the retinal photoreceptors and the signal transmits to the retinal ganglion cells, we then measured outer retinal function, using FERG. As shown in Figure 1C, the amplitude of FERG exhibited a noteworthy reduction as age increased (Factor age, $P<0.001$). However, this decrease did not display any notable distinctions between the groups (Factor Group, $P=0.55$) despite the time course was not completely overlapping (Age x Group, $P=0.003$). Intriguingly, although the decline in FERG amplitude within the study groups was akin to that observed in naïve mice, there was a temporary increase in all study groups at the first post-injection measurement.

Next, to detect if the injection induced any change in retinal structure, we used SD-OCT to quantify the thickness of the inner retinal layers, encompassing the nerve fiber layer (RNFL), ganglion cell layer (RGC), and inner plexiform layer (IPL) (Figure 1D upper panel), as well as the overall retina thickness (Figure 1D lower panel). The GEE analysis showed that both the total and inner retinal thicknesses displayed age-related changes that were comparable to that of the FERG. Specifically, a significant age-related decline was evident (Factor Age, $P<0.001$); however, there is no significant

Preprints (www.preprints.org) | NOT PEER-REVIEWED | Posted: 28 September 2023 doi:10.20944/preprints202309.1961.v1

difference between Groups (Factor Group, P>0.3) and the time course was not overlapping (Age x Group, P< 0.005). Additionally, a transient thickening of the retina was observed across all study groups at the first post-injection measurement, coinciding with an increase in FERG amplitude. This phenomenon could be potentially caused by sterile inflammation, as reported in post-operative cataract patients [27,28].

Then, we determined whether MTSAAV delivered wild type *hND4* could reverse RGC dysfunction induced by mutant *hND4* allele in mice using PERGs, a sensitive electrophysiologic measure for RGC function. Before the intravitreal injection, conducted when the mice were at 3 months of age, no discernible differences were observed in PERG amplitude between the naïve and the injected mice of each group. However, the GEE analysis unveiled a progressive decline in PERG amplitude across all groups, albeit with differing patterns between the groups (effect of age, P <0.001; effect of group, P=0.025; Age x Group, P=0.74).

Post-hoc comparison revealed that the PERG amplitude of the Control group was larger than that of the LHON group (P=0.009), while no substantial difference was noted compared to the Rescue group (P=0.12). It is important to note that the progressive decline in PERG amplitude within the Control group almost coincided with a similar decline observed in naïve mice. This indicates that the age-related decline in PERG amplitude in the control mice was primarily related to physiological decline occurring in DBA/1J mice and was not attributed to the influence of double intravitreal injection of mCherry. However, the double intravitreal injections did lead to a temporary drop in PERG amplitude across all groups at the first post-injection measurement, which subsequently displayed partial recovery in later measurements. Due to the inherent physiological decline, the PERG amplitude of all groups tended to converge at 15 months of age, as the dynamic range of response (the difference between the amplitude in naive mice and noise) decreased with increasing age. In dynamic range units, the group difference at the 15-month time point was substantial; the LHON group exhibited an approximate 40% reduction in normal PERG amplitude, whereas the control and rescue groups maintained a normal amplitude level (Figure 1E).

Furthermore, GEE showed that the PERG latency increased with ages in all study groups (Factor Age, P <0.001, Factor Group, P = 0.57, Age x Group, P= 0.58). Notably, the age-related PERG latency increase in the study groups paralleled a similar increase in the naïve group (Fig.1F)

Collectively, these findings provide compelling evident that intravitreal injection of the mutant hND4 only induce RGC dysfunction, characteristic of LHON disease in humans. Moreover, this induced phenotype appears to be subject to long-term rescue through a subsequent intravitreal injection of the wild type allele.

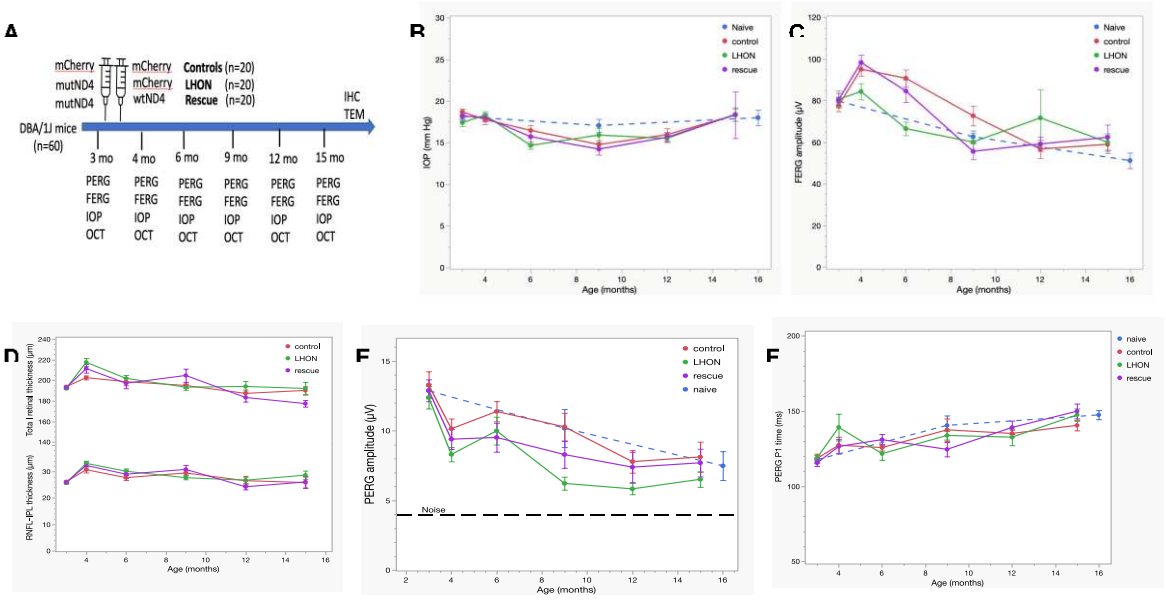

Figure 1. Mito-targeted wtND4 rescue mutND4-induced RGC dysfunction. (**A**) Study design and timeline for the retinal structure and function follow-up. (**B**) Pre-injection and post-injection IOPs

 doi:10.20944/preprints202309.1961.v1

were similar in the study groups. (**C**) FERG amplitudes temporarily increased in all study groups after intravitreal injections and then returned to physiological level. (**D**) Inner retina thickness and total retinal thickness were temporarily increased in all study groups after intravitreal injections and then returned to baseline level (**E**) Pattern ERG amplitudes temporarily decreased in all study groups and progressively recovered the physiological level in control and rescue study groups but not in the LHON group. (**F**) PERG latencies physiologically increased with age in all study groups.

3.2. Wild-type hND4 rescues loss of visual acuity induced by mutant hND4

Visual acuity loss is the most obvious manifestation of LHON. It can be objectively measured in mice using optomotor (OMR) reflex [29,30]. However, less pigmented mice, such as DBA/1J, exhibit a deficiency in their head-tracking response and reflex during Optokinetic tests, likely due to a developmental abnormality in ocular melanin synthesis. This condition leads to retinal underdevelopment and misrouting of the visual pathway [31]. In this study, we opted for a surrogate measure of visual acuity by using the PERG, a method detailed in prior publications [32,33]. PERG responses were recorded at multiple spatial frequencies. As spatial frequency increased, the PERG amplitude exhibited a gradual decline, eventually reaching the threshold of background noise level (signal-to-noise ratio = 1). The intersection of PERG amplitude with the noise level represented the spatial resolution of the retinal output (PERG acuity). As shown in Figure 2A, in a subgroup of mice 15 months old, the PERG-derived visual acuity was 0.242 cy/deg in the control group (n=8), 0.153 cy/deg in the LHON group (n=6), and 0.293 cy/deg in the rescue group (n=6).

Altogether, this experiment unveils a notable visual acuity decrement of approximately 0.2 LogMAR (equivalent to roughly two lines on the Snellen Chart) in LHON mice compared to controls. Importantly, this acuity loss was effectively prevented by the application of wild type hND4 in the rescued group.

3.3. Wild-type hND4 rescues loss of RGC metabolic autoregulation induced by mutant hND4.

It is well-known that flicking light induces rapid dilation of retinal vessels, a phenomenon known as functional hyperemia. Both in mice and humans, this flicker-induced functional hyperemia is associated with an auto-regulatory response of RGCs, consisting in a slow reduction of PERG amplitude to a plateau- an occurrence termed PERG adaptation [24,34,35]. PERG adaptation is found to be compromised in human [36] and mouse glaucoma [37], indicating a deficiency in the ability of RGCs to auto-regulate in response to a metabolically challenging stimulus. In a subgroup of Naïve (n=10), Control (n=7), LHON (n=8) and Rescue (n=8) mice, we have measured flicker-induced PERG adaptation by sequentially recording PERG responses with superimposed flicker at two distinct frequencies: 101 Hz (not detectable) and 11 Hz (visible). As adaptive responses are typically variable, we combined data collected in the post-injection age range of 5-15 months in order to increase the sample size. Figure 2B shows that the transition from non-flicker to flicker produced a marked reduction in PERG amplitude, totaling 33% in Naïve mice and 34% in Control mice, indicating normal autoregulation [24]. In contrast, the LHON group exhibited a loss of flicker adaptation, pointing to a malfunction in the autoregulatory mechanism. Remarkably, in the Rescue group, the restoration of flicker adaptation was achieved to a magnitude of 30%, and this rescue effect was statistically significant (effect of flicker, $P<0.001$, effect of Group, $P=0.004$; Interaction Flicker x Group, $P<0.001$).

Preprints (www.preprints.org) | NOT PEER-REVIEWED | Posted: 28 September 2023 doi:10.20944/preprints202309.1961.v1

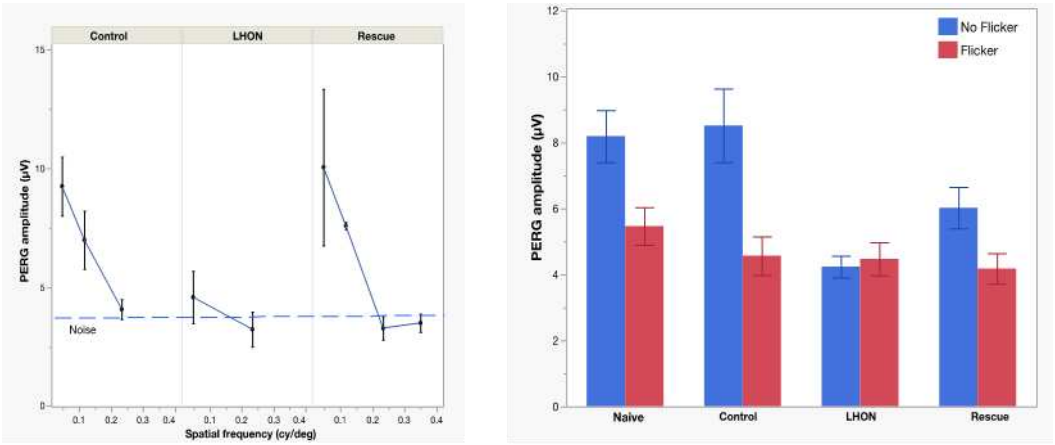

Figure 2. wildtype ND4 improve the visual acuity**.** (**A**) The PERG signal decreases with increasing spatial frequency. The linear extrapolation of PERG amplitude to the noise level represents the retinal acuity, which is higher in the control group (0.242 cy/deg) lowest in the LHON group (0.153 cy/deg), and intermediate in in the rescue group (0.293 cy/deg). (**B**) Flickering light superimposed to the PERG stimulus causes reduction of PERG amplitude (autoregulatory adaptation), which is present in both naïve and control group (34% amplitude change). Flicker adaptation is lost in the LHON group, but it is restored (30%) in the rescue group.

3.4. Wild-type hND4 rescues loss of RGCs induced by mutant hND4.

To further assess the rescue effects of delivered wild type *hND4*, we performed post-mortem histological analysis at 15 months post intravitreal injection. The average density of RBPMS-positive RGCs was quantified in flat mounted retinae in groups of the Naïve (n=3, Figure 3A), Control (n=5, Figure 3B), LHON (n=4, Figure 3C) and Rescue (n=4, Figure 3D). Multiple measures from the same mice were accounted for in the GEE analysis. The effects between the groups was highly significant ($p<0.001$). Specifically, a significant decline in RGC density was evident in the LHON group compared to the control group ($p<0.001$), while RGC density in the Rescue group was similar to that of either Controls or Naïve mice ($P=0.106$, Figure 3E).

To provide visual representations of RGC density distributions across the different groups, we expressed RGC densities collected in all retinal samples as probability density functions. As shown in Figure 3F, RGC distribution of Control mice exhibited an overlap with that of Naïve mice, while the RGC distribution of LHON mice displayed a narrower than that of Control mice and it is markedly shifted towards smaller densities. The RGC distribution of Rescue mice appears to be bimodal, with one subpopulation of RGC densities in the Control range and another subpopulation in the LHON range. Altogether, these results suggest that the delivered wildtype hND4 can rescue, at least in part, the loss of RGCs induced by mutant hND4.

Preprints (www.preprints.org) | NOT PEER-REVIEWED | Posted: 28 September 2023 doi:10.20944/preprints202309.1961.v1

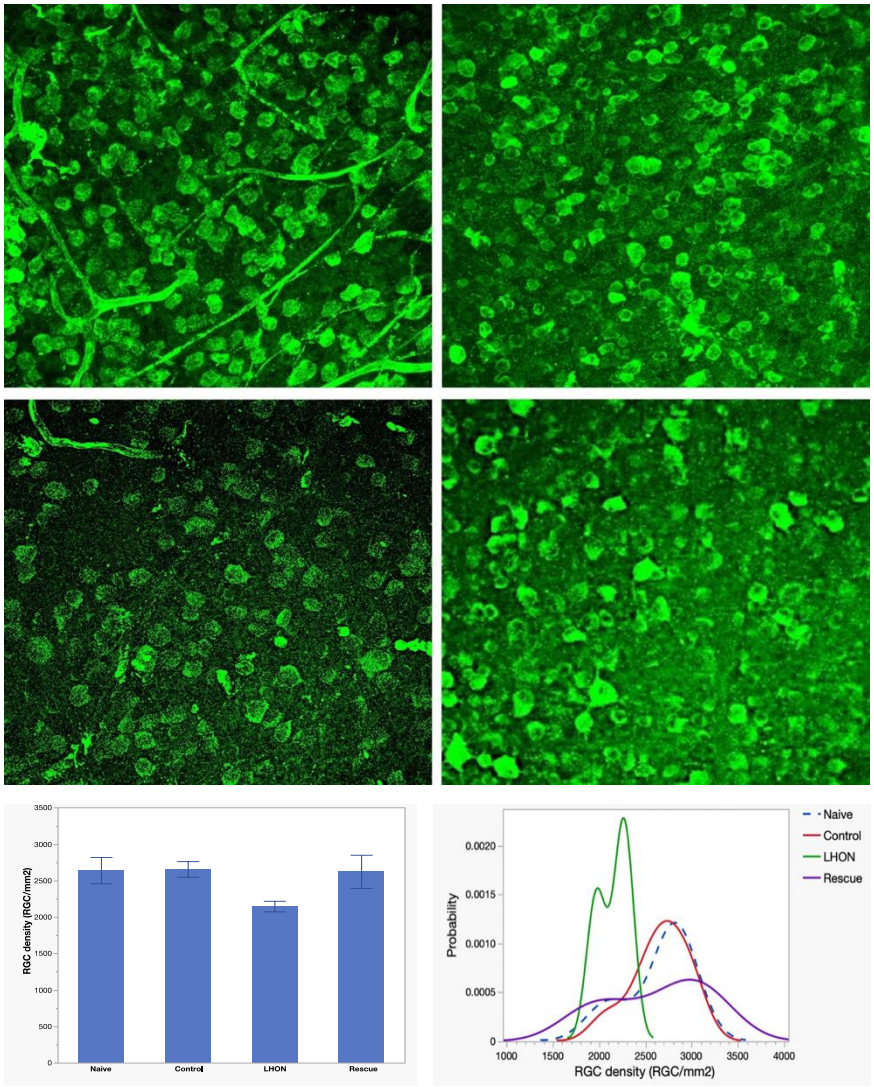

Figure 3. wiltype ND4 prevent RGC loss in LHON mice**.** (**A-D**) Representative immunostaining of retinal whole mount using RBPMS (a pan-RGC marker) showed RGCs distribution in Naïve (**A**), Control (**B**), LHOH (**C**), and Rescued (**D**) mice. (**E**) The mean RGC density at the endpoint is lower in the LHON group compared to naïve, control and rescue groups. (**F**) The probability distribution of RGC density in the LHON group is shifted to the left compared to overlapping distributions of controls and naive groups. The rescue group appears to have a bimodal distribution with one peak in the LHON range and another peak in the range of controls.

3.5. Wild-type hND4 rescues optic atrophy induced by mutant hND4

To evaluate the rescue efficacy of optic atrophy, we performed ultrastructural analysis using transmission electron microscope (TEM) 15 months after intravitreal injection. Three optic nerves were analyzed from each group of the Naïve (Figure 4A), Control (Figure 4B). LHON (Figure 4C), and Rescue (Figure 4D). Axon density was calculated from axon counts on 8 sections of each optic nerve. Since the sample was limited, results were descriptive and expressed as probability density functions of all measurements for each group. We found that distribution of axon density in all study groups were shifted toward smaller axon density, compared to that of age-matched Naïve mice. However, there was no obvious difference in axon density distributions between Control, LHON, and Rescue groups (Fig. 4E).

Preprints (www.preprints.org) | NOT PEER-REVIEWED | Posted: 28 September 2023 doi:10.20944/preprints202309.1961.v1

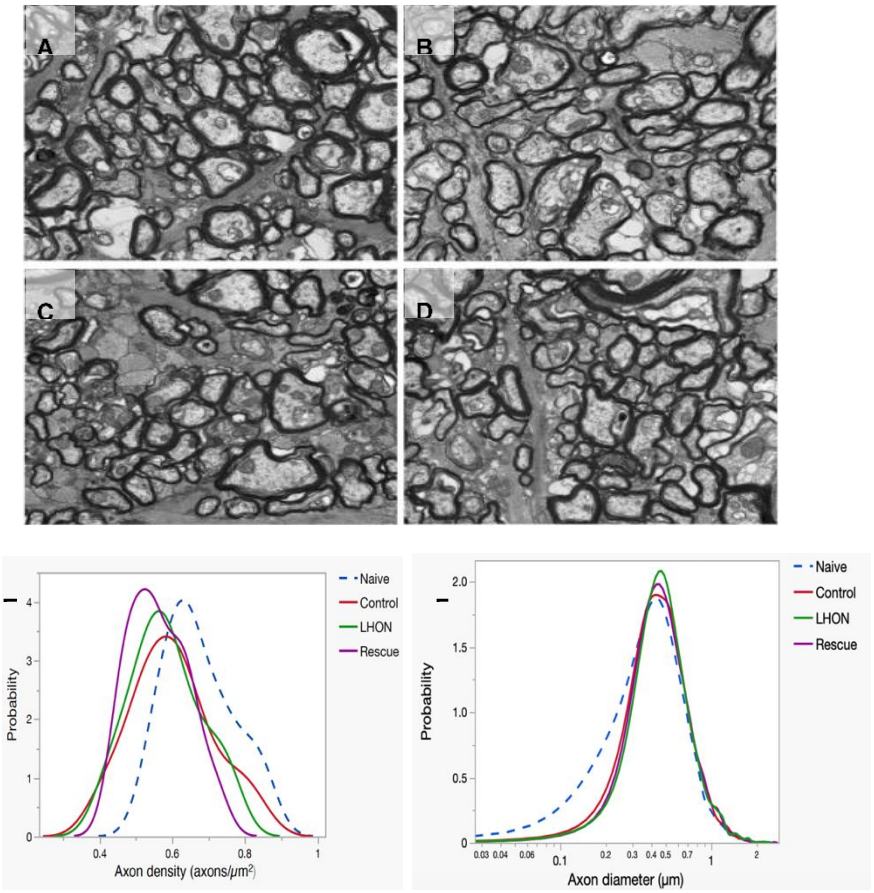

Figure 4. wildype ND4 protect optic nerve degeneration. (**A-D**) Representative transmission electron micrographs of the retrobulbar optic nerve showed the axon distribution in Naïve (**A**), Control (**B**), LHON (**C**), and Rescued (**D**) mice. (**E**) The distribution of axon density shows higher density in the naïve group compared with other three group. (**F**) The main distribution of axon diameter is similar in all groups, but the naïve group has a tail of axons smaller than 0.3 μm.

Next, Axon size was measured on about 2,000 axons of each optic nerve. The distribution of axon size in all study groups had lost a subpopulation of axons smaller than 0.3 μm, compared to that of age-matched Naïve mice. Otherwise, the distribution of axon sizes in Control, LHON, and Rescue groups appears to be very similar (Figure 4F).

To further evaluate the morphological of axons and mitochondria, we used a well-established scoring system previously reported [38–40]. This scoring systme allowed us to assign a "*health score*" to each sample, categorinzing it as follows: 1 (no or minimal changes), 2 (definite but moderate changes), and 3 (severe changes). The Scoring was performed by two independent observers who were blinded to the study groups of the optic nerves. Analysis of both axon (Figure 5A) and mitochondria scores (Figure 5B) clearly demonstrates a higher frequency of moderate to severe ultrastructural changes within the LHON group in comparision to the Naïve and Control groups. However, in the Rescue group, the distribution of health score approached that observed in Naïve and Control mice. Altogether, these results indicate that the wild-type hND4 rescues, at least in part, the ultrastuctural axonal and mitochondrial changes induced by the mutant hND4.

Preprints (www.preprints.org) | NOT PEER-REVIEWED | Posted: 28 September 2023 doi:10.20944/preprints202309.1961.v1

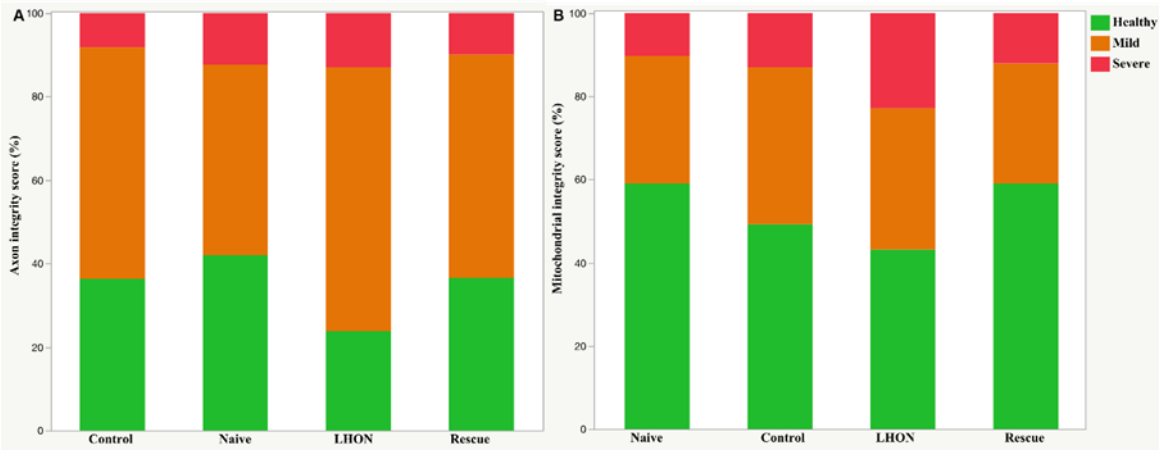

Figure 5. wildtype ND4 preserve mitochondrial and RGC axonal integrity. Integrity scoring for the axon (**A**) and mitochondria in the optic nerve (**B**). LHON rescue group has similar healthy axons and mitochondria with the age control and negative control groups. (N=5 per groups, 15-month-old).

4. Discussion

Current treatments for LHON remain insufficient, leaving the disease without a definitive cure. Several therapeutic strategies are in development to manage LHON, including genetic therapies, antioxidant and neurotrophic therapies, promotion of mitochondrial biogenesis, mitochondrial replacement therapy, and stem cell-based approaches. Among these, allotopic gene therapy has advanced to human clinical trials for the m. 11778G>A mutation in China (NCT01267422) [7], France (NCT02064569) [8], and the USA (NCT02161380). Despite the observation of visual improvement among participants in these clinical trials, the majority of individuals still have low vision, leading them to be categorized as legally blind, especially those who have visual loss for more than one year [8,9,41,42]. This might be due to the hydrophobicity of ND4 protein that is difficult to import and sort across the mitochondrial membrane when produced remotely, such as in cytosol [43–45]. MTS-AAV overcomes these limitations by delivering the gene of interest (ND4) directly into the mitochondria. In this study, we further assessed the rescue efficacy of MTSAAV-delivered wild type hND4 in an LHON mouse model. Our evaluation covers visual acuity, RGC metabolic autoregulation, RGC function, and axon and mitochondria integrity.

PERG spatial resolution has proven to be a valuable tool for assessing visual acuity in wild type and mutant mice [30]. PERG acuity measurements reflect the spatial resolution of the retinal output [49,50] and align with those obtained through other methods, such as Optomotor response (OMR) and pattern visual evoked potential (PVEP) [32]. In this study we used PERG acuity as mice of the DBA strain, as albino mice, do not have an OMR reflex. Our results showed that the PERG acuity of LHON mice was lower the acuity of control mice. However, the PERG acuity of mice rescued with wild type hND4 was similar to the PERG acuity of control mice.

Flickering light increases metabolic demand in the inner retina and induces functional hyperemia [34,35,51]. When flickering light is superimposed to the PERG stimulus, the PERG signal progressively declines to a plateau lower than the initial amplitude by about 30% [24]. PERG adaptation to flicker represents a physiological autoregulatory mechanism that is lost in dysfunctional RGCs [24]. Our results show that flicker-induced PERG adaptation is lost in LHON mice but is regained in rescued mice. These results suggest that wild type hND4 preserved an autoregulatory mechanism of RGCs that depends or retinal metabolism.

In conclusion, we assessed the rescue efficacy of MTSAAV-delivered wild type *hND4* in a LHON mouse model. The delivered gene demonstrated its potential to counteract the harmful effects of mutant *hND4* in mice. Specifically, it displayed the ability to prevent RGC loss, halt RGC dysfunction, restore RGC metabolic autoregulation, uphold visual acuity, and preserve the integrity of axons and

mitochondria. Results from this study will significantly benefit the translation of this mitochondrial targeted approach into future clinical trials for LHON patients carrying *ND4G11778A* mutation.

Author Contributions: V.P., J.G., and H.Y. designed the study. T.C., Z.H., D.E.A., A.L., G.G.A., and J.D.E. conducted the research. T.C., and V.P. conducted the data analysis. and T.C., V.P., and H. Y. wrote and revised the manuscript. All authors have read and agreed to the published version of the manuscript.

Funding: This research was funded by the National Eye Institute R24 EY028785, R01 EY 027414, R01 EY017141, and P30 EY014801 Bascom Palmer Eye Institute Core Grant.

Institutional Review Board Statement: The animal study protocol was approved by the Institutional Review Board of University of Miami. All animal procedures were performed abiding by the National Institutes of Health Guide for Care and Use of Laboratory Animals and the ARVO Statement for the use of Animals in Ophthalmic and Vision Research.

Informed Consent Statement: Not applicable.

Data Availability Statement: The original contributions presented in the study are included in the article/**Supplementary Material**. Further inquiries can be directed to the corresponding authors.

Acknowledgments: The authors acknowledge the defining contributions of John Guy, M.D. (deceased), who invented mito-targeting AAV. His tireless efforts made this study possible. We also gratefully acknowledge Dr. Alfred S. Lewin and Mr. Vince A. Chiodo at the University of Florida for the MTSAAV package.

Conflicts of Interest: The authors declare no conflict of interest.

References

1. Kauppila, J.H.K.; Baines, H.L.; Bratic, A.; Simard, M.L.; Freyer, C.; Mourier, A.; Stamp, C.; Filograna, R.; Larsson, N.G.; Greaves, L.C., et al., A Phenotype-Driven Approach to Generate Mouse Models with Pathogenic mtDNA Mutations Causing Mitochondrial Disease. *Cell Rep.* **2016**, 16(11), p. 2980-2990.
2. Jurkute, N. Yu-Wai-Man, P., Leber hereditary optic neuropathy: bridging the translational gap. *Curr Opin Ophthalmol.* **2017**, 28(5), p. 403-409.
3. Yu-Wai-Man, P.; Griffiths, P.G.; Hudson, G. Chinnery, P.F., Inherited mitochondrial optic neuropathies. *J Med Genet.* **2009**, 46(3), p. 145-58.
4. Bacman, S.R.; Williams, S.L.; Pinto, M.; Peralta, S. Moraes, C.T., Specific elimination of mutant mitochondrial genomes in patient-derived cells by mitoTALENs. *Nat Med.* **2013**, 19(9), p. 1111-3.
5. Yu, H.; Koilkonda, R.D.; Chou, T.H.; Porciatti, V.; Ozdemir, S.S.; Chiodo, V.; Boye, S.L.; Boye, S.E.; Hauswirth, W.W.; Lewin, A.S., et al., Gene delivery to mitochondria by targeting modified adenoassociated virus suppresses Leber's hereditary optic neuropathy in a mouse model. *Proc Natl Acad Sci U S A.* **2012**, 109(20), p. E1238-47.
6. Chadderton, N.; Palfi, A.; Millington-Ward, S.; Gobbo, O.; Overlack, N.; Carrigan, M.; O'Reilly, M.; Campbell, M.; Ehrhardt, C.; Wolfrum, U., et al., Intravitreal delivery of AAV-NDI1 provides functional benefit in a murine model of Leber hereditary optic neuropathy. *Eur J Hum Genet.* **2013**, 21(1), p. 62-8.
7. Liu, H.L.; Yuan, J.J.; Zhang, Y.; Tian, Z.; Li, X.; Wang, D.; Du, Y.Y.; Song, L. Li, B., Factors associated with rapid improvement in visual acuity in patients with Leber's hereditary optic neuropathy after gene therapy. *Acta Ophthalmol.* **2020**, 98(6), p. e730-e733.
8. Yu-Wai-Man, P.; Newman, N.J.; Carelli, V.; Moster, M.L.; Biousse, V.; Sadun, A.A.; Klopstock, T.; Vignal-Clermont, C.; Sergott, R.C.; Rudolph, G., et al., Bilateral visual improvement with unilateral gene therapy injection for Leber hereditary optic neuropathy. *Sci Transl Med.* **2020**, 12(573).
9. Guy, J.; Feuer, W.J.; Davis, J.L.; Porciatti, V.; Gonzalez, P.J.; Koilkonda, R.D.; Yuan, H.; Hauswirth, W.W. Lam, B.L., Gene Therapy for Leber Hereditary Optic Neuropathy: Low- and Medium-Dose Visual Results. *Ophthalmology.* **2017**, 124(11), p. 1621-1634.
10. Lam, B.L.; Feuer, W.J.; Davis, J.L.; Porciatti, V.; Yu, H.; Levy, R.B.; Vanner, E. Guy, J., Leber Hereditary Optic Neuropathy Gene Therapy: Adverse Events and Visual Acuity Results of all Patient Groups. *Am J Ophthalmol.* **2022**.
11. Kaeppel, C.; Beattie, S.; Fronza, R.; van Logtenstein, R.; Salmon, F.; Schmidt, S.; Wolf, S.; Nowrouzi, A.; Glimm, H.; von Kalle, C., et al., AAV Integrates Randomly into the Nuclear and Mitochondrial Genome after LPLD Gene Therapy. *Molecular Therapy.* **2013**, 21, p. S104-S105.
12. Yu, H.; Koilkonda, R.D.; Chou, T.H.; Porciatti, V.; Ozdemir, S.S.; Chiodo, V.; Boye, S.L.; Boye, S.E.; Hauswirth, W.W.; Lewin, A.S., et al., Gene delivery to mitochondria by targeting modified adenoassociated virus suppresses Leber's hereditary optic neuropathy in a mouse model. *Proceedings of the National Academy of Sciences of the United States of America.* **2012**, 109(20), p. E1238-E1247.

13. Yu, H.; Ozdemir, S.S.; Koilkonda, R.D.; Chou, T.H.; Porciatti, V.; Chiodo, V.; Boye, S.L.; Hauswirth, W.W.; Lewin, A.S. Guy, J., Mutant NADH dehydrogenase subunit 4 gene delivery to mitochondria by targeting sequence-modified adeno-associated virus induces visual loss and optic atrophy in mice. *Mol Vis.* **2012**, 18, p. 1668-83.
14. Yu, H.; Koilkonda, R.D.; Chou, T.H.; Porciatti, V.; Mehta, A.; Hentall, I.D.; Chiodo, V.A.; Boye, S.L.; Hauswirth, W.W.; Lewin, A.S., et al., Consequences of zygote injection and germline transfer of mutant human mitochondrial DNA in mice. *Proc Natl Acad Sci U S A.* **2015**, 112(42), p. E5689-98.
15. Liu, Y.; Eastwood, J.D.; Alba, D.E.; Velmurugan, S.; Sun, N.; Porciatti, V.; Lee, R.K.; Hauswirth, W.W.; Guy, J. Yu, H., Gene therapy restores mitochondrial function and protects retinal ganglion cells in optic neuropathy induced by a mito-targeted mutant ND1 gene. *Gene Ther.* **2022**.
16. Yu, H.; Sant, D.W.; Wang, G. Guy, J., Mitochondrial Transfer of the Mutant Human ND6T14484C Gene Causes Visual Loss and Optic Neuropathy. *Transl Vis Sci Technol.* **2020**, 9(11), p. 1.
17. Velmurugan, S.; Chou, T.H.; Eastwood, J.D.; Porciatti, V.; Liu, Y.; Hauswirth, W.W.; Guy, J. Yu, H., Comparison of different gene-therapy methods to treat Leber hereditary optic neuropathy in a mouse model. *Front Neurosci.* **2023**, 17, p. 1119724.
18. Chou, T.H.; Bohorquez, J.; Toft-Nielsen, J.; Ozdamar, O. Porciatti, V., Robust Mouse Pattern Electroretinograms Derived Simultaneously From Each Eye Using a Common Snout Electrode. *Investigative Ophthalmology & Visual Science.* **2014**, 55(4), p. 2469-2475.
19. Porciatti, V., The mouse pattern electroretinogram. *Doc Ophthalmol.* **2007**, 115(3), p. 145-53.
20. Yang, X.; Chou, T.H.; Ruggeri, M. Porciatti, V., A new mouse model of inducible, chronic retinal ganglion cell dysfunction not associated with cell death. *Invest Ophthalmol Vis Sci.* **2013**, 54(3), p. 1898-904.
21. Abramoff, M.D.; Garvin, M.K. Sonka, M., Retinal imaging and image analysis. *IEEE Rev Biomed Eng.* **2010**, 3, p. 169-208.
22. Dysli, C.; Enzmann, V.; Sznitman, R. Zinkernagel, M.S., Quantitative Analysis of Mouse Retinal Layers Using Automated Segmentation of Spectral Domain Optical Coherence Tomography Images. *Translational Vision Science & Technology.* **2015**, 4(4).
23. Braha, M.; Porciatti, V. Chou, T.H., Retinal and cortical visual acuity in a common inbred albino mouse. *Plos One.* **2021**, 16(5).
24. Chou, T.H.; Toft-Nielsen, J. Porciatti, V., Adaptation of retinal ganglion cell function during flickering light in the mouse. *Sci Rep.* **2019**, 9(1), p. 18396.
25. Fan, Q.; Teo, Y.Y. Saw, S.M., Application of advanced statistics in ophthalmology. *Invest Ophthalmol Vis Sci.* **2011**, 52(9), p. 6059-65.
26. Zeger, S.L. Liang, K.Y., An overview of methods for the analysis of longitudinal data. *Stat Med.* **1992**, 11(14-15), p. 1825-39.
27. Lietze, A., The role of particulate insoluble substances in food allergy. 3. Heat labile antibody to wheat starch in sera of wheat sensitive patients. *Ann Allergy.* **1969**, 27(1), p. 9-12.
28. Sadowsky, C.; Muhl, Z.F.; Sakols, E.I. Sommerville, J.M., Temporomandibular joint sounds related to orthodontic therapy. *J Dent Res.* **1985**, 64(12), p. 1392-5.
29. Shi, C.; Yuan, X.; Chang, K.; Cho, K.S.; Xie, X.S.; Chen, D.F. Luo, G., Optimization of Optomotor Response-based Visual Function Assessment in Mice. *Sci Rep.* **2018**, 8(1), p. 9708.
30. Kretschmer, F.; Sajgo, S.; Kretschmer, V. Badea, T.C., A system to measure the Optokinetic and Optomotor response in mice. *J Neurosci Methods.* **2015**, 256, p. 91-105.
31. Jeffery, G.; Brem, G. Montoliu, L., Correction of retinal abnormalities found in albinism by introduction of a functional tyrosinase gene in transgenic mice and rabbits. *Brain Res Dev Brain Res.* **1997**, 99(1), p. 95-102.
32. Braha, M.; Porciatti, V. Chou, T.H., Retinal and cortical visual acuity in a common inbred albino mouse. *PLoS One.* **2021**, 16(5), p. e0242394.
33. Porciatti, V.; Pizzorusso, T.; Cenni, M.C. Maffei, L., The visual response of retinal ganglion cells is not altered by optic nerve transection in transgenic mice overexpressing Bcl-2. *Proc Natl Acad Sci U S A.* **1996**, 93(25), p. 14955-9.
34. Riva, C.E.; Logean, E. Falsini, B., Visually evoked hemodynamical response and assessment of neurovascular coupling in the optic nerve and retina. *Prog Retin Eye Res.* **2005**, 24(2), p. 183-215.
35. Albanna, W.; Kotliar, K.; Luke, J.N.; Alpdogan, S.; Conzen, C.; Lindauer, U.; Clusmann, H.; Hescheler, J.; Vilser, W.; Schneider, T., et al., Non-invasive evaluation of neurovascular coupling in the murine retina by dynamic retinal vessel analysis. *PLoS One.* **2018**, 13(10), p. e0204689.
36. Monsalve, P.; Triolo, G.; Toft-Nielsen, J.; Bohorquez, J.; Henderson, A.D.; Delgado, R.; Miskiel, E.; Ozdamar, O.; Feuer, W.J. Porciatti, V., Next Generation PERG Method: Expanding the Response Dynamic Range and Capturing Response Adaptation. *Transl Vis Sci Technol.* **2017**, 6(3), p. 5.
37. Chou, T.H.; Romano, G.L.; Amato, R. Porciatti, V., Nicotinamide-Rich Diet in DBA/2J Mice Preserves Retinal Ganglion Cell Metabolic Function as Assessed by PERG Adaptation to Flicker. *Nutrients.* **2020**, 12(7).

38. Cepurna, W.O.; Kayton, R.J.; Johnson, E.C. Morrison, J.C., Age related optic nerve axonal loss in adult Brown Norway rats. *Exp Eye Res.* **2005**, 80(6), p. 877-84.
39. Deng, W.; Hedberg-Buenz, A.; Soukup, D.A.; Taghizadeh, S.; Wang, K.; Anderson, M.G. Garvin, M.K., AxonDeep: Automated Optic Nerve Axon Segmentation in Mice With Deep Learning. *Transl Vis Sci Technol.* **2021**, 10(14), p. 22.
40. Zhu, Y.; Pappas, A.C.; Wang, R.; Seifert, P.; Sun, D. Jakobs, T.C., Ultrastructural Morphology of the Optic Nerve Head in Aged and Glaucomatous Mice. *Invest Ophthalmol Vis Sci.* **2018**, 59(10), p. 3984-3996.
41. Guy, J.; Feuer, W.J.; Porciatti, V.; Schiffman, J.; Abukhalil, F.; Vandenbroucke, R.; Rosa, P.R. Lam, B.L., Retinal ganglion cell dysfunction in asymptomatic G11778A: Leber hereditary optic neuropathy. *Invest Ophthalmol Vis Sci.* **2014**, 55(2), p. 841-8.
42. Yuan, J.; Zhang, Y.; Liu, H.; Wang, D.; Du, Y.; Tian, Z.; Li, X.; Yang, S.; Pei, H.; Wan, X., et al., Seven-Year Follow-up of Gene Therapy for Leber's Hereditary Optic Neuropathy. *Ophthalmology.* **2020**, 127(8), p. 1125-1127.
43. Johnston, I.G. Williams, B.P., Evolutionary Inference across Eukaryotes Identifies Specific Pressures Favoring Mitochondrial Gene Retention. *Cell Syst.* **2016**, 2(2), p. 101-11.
44. Allen, J.F., Why chloroplasts and mitochondria retain their own genomes and genetic systems: Colocation for redox regulation of gene expression. *Proc Natl Acad Sci U S A.* **2015**, 112(33), p. 10231-8.
45. Adams, K.L. Palmer, J.D., Evolution of mitochondrial gene content: gene loss and transfer to the nucleus. *Mol Phylogenet Evol.* **2003**, 29(3), p. 380-95.